American Mineralogist, Volume 86, pages 66–79, 2001

Structural properties of ferromagnesian cordierites

THOMAS MALCHEREK,[1,*] M. CHIARA DOMENEGHETTI,[1] VITTORIO TAZZOLI,[1] LUISA OTTOLINI,[1] CATHERINE MCCAMMON,[2] AND MICHAEL A. CARPENTER[3]

[1]CNR-CSCC, c/o Dipartimento di Scienze della Terra, Via Ferrata 1, 27100 Pavia, Italy
[2]Bayerisches Geoinstitut, Universität Bayreuth, D-95440 Bayreuth, Germany
[3]Department of Earth Sciences, University of Cambridge, Downing Street, Cambridge CB2 3EQ, U.K.

ABSTRACT

A set of natural and heat-treated cordierite crystals has been analyzed using single-crystal X-ray diffraction, EMPA, SIMS, and ^{57}Fe Mössbauer-spectroscopy. Structure determination of natural cordierite shows that the average size of the tetrahedrally coordinated $T_1$1 cation increases systematically by about 0.01 Å as the Fe content of the solid solution decreases toward the Mg end-member. For Fe-rich compositions, the mean tetrahedral bond length $T_1$1-O is close to 1.749 Å, a value expected for an AlO_4 tetrahedron in an alumosilicate framework structure. It is suggested that the structural dilation of the tetrahedral sites, which is driven by the decreasing average size of the octahedral cation, is sustained by substitution of the large cations Mg and Fe^{2+} for Al. Mössbauer spectroscopy shows that up to 11% of Fe^{2+} can be attributed to tetrahedral coordination in Mg-rich cordierite. Charge balance for the substitutions is either provided by introduction of Na^+ into vacant Ch2(0,0,0) channel sites or by substitution of an additional Al^{3+} by Si^{4+}. Tetrahedral site occupancies and corresponding Al,Si order parameters are calculated on the basis of a simple hard sphere model, based on refined cation-oxygen mean bond length, chemical composition, and Fe site-occupancy refinements. Almost complete Al,Si ordering among ring sites T_2 is encountered for most natural cordierite samples. Al,Si ordering among the T_1 tetrahedra is less pronounced for Fe-rich compositions. Partial disorder is attributable to Al/Si ratios in excess of 4/5. Orthorhombic shear strain is shown to correlate with the derived average order parameter, if corrections for strain contributions from size effects of the octahedral cation and from channel constituents are employed. Crystal-chemical similarities to other compounds and the implications of the minor cation substitutions for the properties of structural phase transitions in cordierite are discussed.

INTRODUCTION

In nature, cordierite occurs predominantly in its orthorhombic low-temperature modification, SG symmetry *Cccm* (Gibbs 1966), with idealized composition $(Mg,Fe)_2[Al_4Si_5O_{18}]$. Almost all natural cordierites deviate from this ideal composition and contain substantial amounts of Na and volatile molecules such as H_2O or CO_2.

The high-temperature modification of cordierite, indialite, or high-cordierite, is known to have hexagonal symmetry and a disordered Al,Si configuration. The indialite structure is isotypic with that of beryl and has space group symmetry *P6/mcc* (Meagher and Gibbs 1977).

The structure of ferromagnesian cordierites has been the subject of numerous studies (Gibbs 1966; Cohen et al. 1977; Hochella et al. 1979; Wallace and Wenk 1980; Armbruster 1985c, 1986), however, many aspects of its crystal chemistry remain unclear. The aim of this work is to examine the structural controls of cation substitutions and Al,Si ordering in the tetrahedral framework of Fe,Mg-cordierites, and to re-analyze the various causes for orthorhombic lattice distortion (orthorhombic shear strain) in low-cordierites.

* Present address: Institut für Mineralogie, Corrensstrasse 24, 48149 Münster, Germany. E-mail: malcher@nwz.uni-muenster.de

The structural topology of cordierite

Two types of topologically different tetrahedra can be distinguished in the cordierite structure: T_1 tetrahedra share two opposite edges with octahedra that coordinate the *M*-cation. These edge-sharing tetrahedra and octahedra form infinite, honeycomb-structured layers normal to the crystallographic *c*-axis (M-layers). Distorted hexagonal rings of corner-sharing T_2 tetrahedra (T-layers) are found between the M-layers, inscribed into their large openings. Each T_2 tetrahedron shares two corners with T_1-tetrahedra in M-layers above and below it. In this way, each T_1 tetrahedron connects two T_2-rings beneath an M-layer to two others above it. The T_2-rings are contra-rotated by ca. 30° in adjacent T-layers, giving rise to two different types of T-layers and to a **c**-repeat comprising two M-layers and both T-layers. Thus an infinite stack of T_1 tetrahedra is formed parallel to the **c**-axis.

The M-layer building block is not only found in the structures of beryl and cordierite. In the milarite structure, the M-layers combine with contra-rotated layers of tetrahedral double rings, thus increasing the **c** lattice dimension relative to the beryl structure. Hawthorne et al. (1991) list 14 minerals associated with this structure type. In the context of the present work, the structure of merrihueite $(K,Na)_2(Fe,Mg)_2[(Fe,Mg)_3Si_{12}O_{30}]$ (Khan et al. 1972 and references cited therein) will be of particular interest.

The framework of corner-sharing tetrahedra, a feature common to all of these structures, leaves open channels parallel to [001]. Larger cavities along these channels may contain molecules, such as H_2O or CO_2, or large cations such as K^+. The volatile molecules can be reversibly removed from these cavities via heating (Armbruster and Bloss 1982; Armbruster 1985a; Vry et al. 1990). At the openings of the cavities, six-membered rings of oxygen anions form a "bottleneck." Na^+ partially occupies the center of these rings, giving rise to a non-homogeneous contraction of the bottleneck and a simultaneous increase in the b-lattice dimension (Armbruster 1986). As a result the distortion index, $\Delta = 1.094 \cdot (a - b\sqrt{3})$ (Putnis 1980; Selkregg and Bloss 1980), decreases in Na-rich cordierites. In hydrous cordierites, the Na-cation is coordinated by two water molecules situated in the channel cavities above and below it (Type II water, cf. Armbruster 1985a). In anhydrous cordierite, these water molecules are absent and the Na-cation therefore shows increased thermal motion along the channel axis (Armbruster 1986).

The site nomenclature outlined by Cohen et al. (1977) is followed here. The three T_1 tetrahedra in the M-layers are subdivided into two T_11 and one T_16 site, whereas the six T_2 tetrahedra are labeled T_21, T_23, and T_26, with each of the latter sites occurring twice. In the ordered structure of orthorhombic $Mg_2Al_4Si_5O_6$, these sites are filled by Al, Si, Si, Si, and Al, respectively.

Cation substitutions in tetrahedral sites

The possibility of Be occurring in cordierite is particularly compelling given the isomorphy of indialite and beryl, $Al_2[Be_3Si_6O_{18}]$. Beryllium occupies all of the T_1 tetrahedra in the idealized structure of beryl, whereas the T_2 tetrahedra are filled exclusively by Si. In spite of the structural similarity between the two minerals, only limited solid solubility (ca. 4 mol% beryl in cordierite) has been obtained experimentally (Povondra and Langer 1971a). On the other hand, appreciable Be-concentrations have been found in natural cordierites of pegmatitic origin, which are almost invariably Na-rich. This suggests the substitution scheme $Be^{2+} + Na^+ = Al^{3+}$ to be operating in these minerals. Experimental studies by Povondra and Langer (1971b) confirmed NaBe cordierites with as much as 16% of Al substituted by Be at 3 kbar and 700 °C. In some natural cordierites up to 10% substitution has been observed (Povondra et al. 1984). Another possible substitution that has been verified experimentally (Schreyer 1985) is $Be^{2+} + Si^{4+} = 2Al^{3+}$, leading to a theoretical end-member $Mg_2[BeAl_2Si_6O_{18}]$. In structural refinements of Be-rich natural cordierites, Armbruster (1986) assigned Be to the T_11 position.

Circumstantial evidence indicates the limited substitution of Mg into the tetrahedral framework of Mg-cordierites. In extreme cases, this leads to compositions with more than two Mg atoms pfu (e.g., Armbruster 1985b). The substitution $Mg^{2+} + Si^{4+} = 2Al^{3+}$ has been postulated by several authors (cf. Schreyer 1985), and, although the theoretical end-member $Mg_2[MgAl_2Si_6O_{18}]$ could not be synthesized, substantial incorporation of excess Mg at high temperatures has been described by Schreyer and Schairer (1961). In natural cordierites, the presence of Na^+ alternatively allows the substitution scheme $Mg^{2+} + Na^+ = Al^{3+}$ to occur. The most likely position to be partially occupied by Mg^{2+} is the T_11 site, where it would replace the smaller Al-cation. The ionic radius of $r = 0.57$ Å (Shannon 1976) for $^{[4]}$Mg is considerably larger than that of Al ($r = 0.39$ Å). However, in the synthetic milarite compound $K_2Mg_2[Mg_3Si_{12}O_{30}]$ (Khan et al. 1972), all of the tetrahedra corresponding to T_1 in the cordierite structure are occupied by Mg, with O-T-O bond angles similar to those of the T_1-site in typical Mg-cordierite, e.g., the White Well cordierite described by Cohen et al. (1977).

Fe^{2+} in tetrahedral coordination is only marginally larger than $^{[4]}$Mg ($r = 0.63$ Å). Hence the above substitution scheme could be written $(Fe,Mg)^{2+} + Si^{4+} = 2Al^{3+}$. Contrary to the case of Mg, there is direct evidence that Fe^{2+} indeed occurs in tetrahedral coordination in natural cordierites. Vance and Price (1984) concluded from Mössbauer and optical spectroscopy on natural samples that minor amounts of Fe^{2+} occur in a tetrahedrally coordinated site, substituting for Al^{3+}. These authors contradicted the earlier conclusions of Goldman and Rossman (1977) who assumed that the non-octahedral Fe occupies channel positions. Recently, Geiger et al. (2000) associated $^{[4]}$Fe with the T_11 site using various spectroscopic techniques and single-crystal X-ray diffraction.

Experimental methods

Heat treatment

To remove volatile molecules from the channel cavities, batches of the cordierite sample each weighing 20–30 mg were wrapped in Pt-foil and annealed at 1173 K. Oxygen fugacity was kept at a level close to that of the QFM buffer ($\log f_{O_2} \approx -13.5$) by using an appropriate H_2/CO_2 mixture controlled by a Tylan RO28 gas mixing valve.

X-ray diffraction

Powder diffraction. Diffraction patterns were recorded using a HUBER G600 Guinier diffractometer with monochromatic Cu$K\alpha_1$ radiation in transmission. Si powder was admixed to the sample material to serve as an internal standard. Lattice constants were determined by full profile fitting using the Rietveld software GSAS (Larson and Von Dreele 1994) and utilizing a profile function with peak asymmetry correction for axial divergence (Finger et al. 1994). Lattice constants of samples SN7289 and SN7225 were obtained from refinement of cordierite mixed with other phases (see Appendix for sample descriptions). Minor amounts of additional phases were also present in the refinements of samples 1997-1 and Zimb.

Single-crystal XRD. Single crystals for X-ray intensity data measurements were selected from the natural and the heated material on the basis of optical clarity, homogeneity, and freedom from inclusions. Extremely thin, oriented lamellar inclusions occurred in two of the natural samples (1997-1 and Great Bear Lake), and the presence of some of these lamellae could not be avoided in the selected single crystals. However, the volume fraction of the lamellae was well below the detection limit in the powder diffraction measurements. The lamellae disappeared after heating to 900 °C. Only very small crystals were available for sample 111249. As a result, the quality of the corresponding refinements is rather poor, compared with those of other crystals. X-ray diffraction was carried out using

TABLE 1. Sample and single-crystal data refinement details for natural and heat treated cordierites

Natural samples	1997-1	126231	ZIMB	1960728	85131	NH1
Heated samples	900 °C in air	900 °C	900 °C	900 °C	900 °C	900 °C
a (Å)	17.0568(8)	17.0645(5)	17.0807(4)	17.0994(7)	17.0987(5)	17.1090(4)
	17.071(2)	17.089(6)[1]	17.096(5)[1]	17.119(5)[1]	17.1135(15)	17.131(3)
b (Å)	9.7154(4)	9.7281(3)	9.7307(3)	9.7358(4)	9.7388(3)	9.7423(3)
	9.717(1)	9.729(4)[1]	9.729(2)[1]	9.735(2)[1]	9.7359(8)	9.744(2)
c (Å)	9.3472(4)	9.3515(2)	9.3427(2)	9.3360(4)	9.3347(3)	9.3318(2)
	9.3479(9)	9.350(7)[1]	9.342(3)[1]	9.334(3)[1]	9.3330(6)	9.3262)
V (Å^3)	1549.0(2)	1552.4(1)	1552.8(1)	1554.2(1)	1554.4(1)	1555.4(1)
	1550.6(2)	1554.5(5)	1553.9(4)	1555.5(4)	1555.0(2)	1556.8(3)
Δ	0.25078	0.23514	0.24794	0.25873	0.25228	0.25692
	0.26448	0.26087	0.26814	0.28090	0.27397	0.27733
μ(cm^{-1})	8.69	10.08	10.67	11.88	11.92	13.115
r_{eqv}(cm)	0.019	0.02	0.018	0.019	0.021	0.015
	0.022	0.025	0.021	0.024	0.017	
No. of unique refl.	2522	2533	2529	2526	2471	2531
	2519	2530	2533	2534	2527	
No. of parameters	90	91	88	88	89	91
	85	84	84	85	85	
isotr. Ext. param.	0.00062	n.r.	n.r.	n.r.	n.r.	n.r.
	n.r.	n.r.	n.r.	n.r.	n.r.	
R_{int}	0.017	0.023	0.0228	0.0231	0.0146	0.0224
	0.0158	0.0126	0.0153	0.0186	0.0233	
R_1 [$F_o > 4\sigma(F_o)$]	0.0188	0.0201	0.0214	0.0221	0.0195	0.0220
	0.0178	0.0168	0.0184	0.0190	0.0205	
R_1(all)	0.0281	0.0328	0.0353	0.0378	0.0262	0.0367
	0.0277	0.0219	0.0265	0.0288	0.0297	
*wR*2	0.0423	0.0435	0.0466	0.0477	0.0414	0.0473
	0.0395	0.0357	0.0400	0.0410	0.0466	
Σ	0.719	0.713	0.692	0.665	0.764	0.712
	0.71	0.778	0.720	0.716	0.738	
weighting coeff. *a*	0.0243	0.0222	0.0243	0.0241	0.0260	0.0228
	0.0224	0.0247	0.0239	0.0221	0.0243	
δe_{max} (Å^{-3})	0.45	0.58	0.55	0.58	0.41	0.62
	0.46	0.61	0.41	0.44	0.55	
δe_{min} (Å^{-3})	–0.44	–0.52	–0.41	–0.38	–0.39	–0.38
	–0.37	–0.27	–0.38	–0.31	–0.45	

Notes: Lattice constants marked [1] have been determined on the single crystals, while for the remaining samples more accurate determinations using Guinier powder diffraction data are available. n.r. = not refined.

a Philips PW1100 4-circle diffractometer with Mo*K*α radiation. Reflections were measured in ω-2θ-scan mode with scan speeds between 0.08 and 0.11 °/s and scan widths between 2.4 and 3.0°, chosen according to crystal size and quality. A quarter Ewald sphere was measured for each crystal, with indices $-32 \le h \le 32$, $0 \le k \le 18$, and $0 \le l \le 17$. Reflections systematically absent due to C-centering were not measured.

The resulting intensity data were generally not corrected for absorption effects, as absorption was deemed negligible (cf. Table 1). Refinements were carried out using the program Shelxl (Sheldrick 1997). A semiempirical isotropic extinction parameter was refined if indicated by large negative differences between observed and calculated structure factors of strong reflections. Scattering factors were chosen for nominally charged atoms, and the real and imaginary parts of the anomalous dispersion correction were included for all atoms. To reduce the effects of discrepancies between the model of nominally charged, spherical ions and the real electron densities, intensities measured at small scattering angles were systematically weighted down by a factor $1 - \exp[-5(\sin\theta/\lambda)^2]$.

Channel water was estimated for untreated crystals by sof-refinement of an uncharged oxygen atom on the 0,0,1/4 (Ch1) position (Table 2)[1]. Sodium was refined at the 0,0,0 (Ch2) position in all crystals. Heated crystals invariably showed an extremely large U_{33} component (Table 3)[1] due to unrestrained thermal motion of Na in the z-direction. A relatively large U_{33} component was also obtained for the nearly H_2O-free natural sample 111249. No residual electron density was observed in the heated crystals at the Ch1-position. After the initial refinement with an oxygen atom situated in 0,0,1/4, two untreated crystals (126231 and NH1) clearly showed a bone-shaped electron density residual oriented along [100] across this position in difference Fourier maps. This electron density residual was interpreted as stemming from a CO_2 molecule and refined subsequently by placing an O atom in x,0,1/4 and a C atom in 0,0,1/4 with equal occupancy. Similar, albeit weaker, residual electron density after the initial refinement also indicated the presence of CO_2 in the GBL sample. In this case, however, the concentration was too small to permit an unrestrained refinement of the O x-coordinate, and the intramolecular C-O distance was therefore held at 1.05 Å. With the exception of high Li contents found in the three most Fe-rich samples (Table 4), all site occupancy factors were refined without chemical constraints to obtain additional information on the crystal chemistry. The results of the structure refinements were combined with the results of the chemical analysis in a subsequent minimization procedure.

[1]For a copy of Tables 2 and 3, document item AM-00-061, contact the Business Office of the Mineralogical Society of America (see inside front cover of recent issue) for price information. Deposit items may also be available on the American Mineralogist web site (http://www.minsocam.org or current web address).

TABLE 1—*Extended*

GBL 900°C	94755 900°C	111249 900°C	GREB370	1997-2 900°C	G13994 900°C
17.1159(5)	17.1178(6)	17.1706(9)	17.1735(7)	17.2142(7)	17.2232(9)
17.132(3)	17.138(5)[1]	17.172(2)		17.248(4)[1]	17.243(1)
9.7458(3)	9.7525(4)	9.7672(5)	9.7859(4)	9.8264(4)	9.8261(5)
9.744(2)	9.751(2)[1]	9.7660(8)		9.821(2)[1]	9.8220(6)
9.3305(3)	9.3301(3)	9.3140(5)	9.3113(3)	9.3027(3)	9.2989(4)
9.330(2)	9.328(3)[1]	9.3142(7)		9.304(3)[1]	9.3020(5)
1556.4(1)	1557.6(1)	1562.0(2)	1564.8(1)	1573.6(1)	1573.7(2)
1557.4(3)	1558.9(4)	1562.0(2)		1576.0(3)	1575.4(2)
0.25783	0.24722	0.27713	0.24486	0.21265	0.22306
0.28002	0.27126	0.28082		0.26040	0.25249
13.87	13.49	17.14	19.29	22.82	23.207
0.018	0.015	0.01	0.018	0.023	0.016
0.015	0.017	0.011		0.018	
2534	2535	2532	2550	2568	2553
2527	2540	2548		2571	
89	89	85	90	90	90
83	84	82		86	
n.r.	n.r.	n.r.	n.r.	0.00992	0.00271
0.000588	n.r.	0.00263		0.00043	
0.0267	0.0321	0.0581	0.0325	0.0197	0.0213
0.0344	0.0228	0.0492		0.0157	
0.0239	0.0262	0.0342	0.027	0.020	0.0222
0.0226	0.0236	0.0319		0.0169	
0.0364	0.0520	0.0902	0.048	0.0268	0.0344
0.0360	0.0380	0.0748		0.0251	
0.0514	0.0546	0.0745	0.0586	0.0448	0.0493
0.0491	0.0501	0.0696		0.0368	
0.723	0.650	0.631	0.685	0.756	0.694
0.694	0.702	0.623		0.707	
0.0279	0.0209	0.0232	0.0225	0.0267	0.0284
0.0193	0.0239	0.0214		0.0236	
0.55	0.64	0.61	0.74	0.50	0.83
0.54	0.72	0.65		0.64	
–0.58	–0.44	–0.7	–0.42	–0.61	–0.56
–0.43	–0.36	–0.49		–0.32	

Chemical analysis

Electron microprobe analysis (EMPA). Following the X-ray intensity data measurements, the single crystals were embedded in epoxy, ground, and polished. For sample GREB370, different crystals had to be used for EMPA and XRD. EMPA was performed on the natural and on selected heat-treated crystals using a CAMECA SX50 microprobe, operating at 20 kV with 3 nA sample current. A wide beam (>10 μm) was used to minimize beam damage during the analysis. All elements were determined by energy dispersive analysis using a Link AN10000 system with ZAF4/FLS quantitative software. The average compositions obtained from analysis of up to 10 points, equally spread across each crystal, are given in Table 4.

Secondary ion mass spectrometry. To check for the presence of light elements secondary ion mass spectrometry (SIMS) was carried out on the natural samples using a Cameca IMS 4f ion microprobe (CNR-CSCC, Pavia) (cf. Table 4). With the exception of samples 111249, Zimb, NH1, GREB370, and 85131, crystals other than those of the above experiments were used for this type of analysis. The experimental procedure is similar to that described by Ottolini et al. (1993), which employs the use of a $^{16}O^-$ primary-ion beam of 5 nA current intensity and ~10 μm diameter, accelerated by –12.5 kV. To reduce matrix effects, medium- to high-energy (~75–125 eV) secondary ions were selected by applying a voltage offset of –100 V to the secondary ion accelerating voltage (+4500 V) on the sample surface, with an energy-slit width of 50 eV. Lithium, Be, and B were detected at masses 7, 9, and 11 amu, respectively. $^{30}Si^+$ was used as the matrix-reference isotope. The quantification was done by means of the empirical approach of working curves via calibration with standards. Because the relative-to-Si ion yields for Li, within this emission-energy range, correlate with the silica content of the matrix (Ottolini et al. 1993), an empirical correction was made to account for residual matrix effects, similar to that described by Černý et al. (1997). No corrections were made for Be and B. Under these circumstances, the accuracy of SIMS analysis is estimated to better than 10% rel. The data in Table 4 are averaged over up to four measurements.

The H_2O concentration was measured by SIMS in three cordierite crystals. The crystal mounts together with the selected cordierite standards (Great Bear and Manitouwadge) were left to degas under the rotary-pump vacuum for a few days, then the samples were analyzed in the ion microprobe sample chamber under the experimental setup developed for H in silicates (Ottolini et al. 1995). The H^+ and $^{30}Si^+$ positive secondary ions were monitored after achieving steady state-sputtering conditions (after about 9 min sputtering time). The accuracy of the H analysis is similar to that of other light elements.

Mössbauer spectroscopy

Mössbauer spectra were recorded at room temperature (293 K) in transmission mode on a constant acceleration spectrometer with a nominal 50 mCi ^{57}Co source in a 6 μm Rh matrix.

TABLE 4. Chemical analysis of natural and heat treated cordierite single crystals

	1	2	2a	3	4	4a	5	6	7	7a	8
SiO_2	49.30	48.51	50.22	48.46	48.21	48.92	48.26	47.60	47.99	49.32	47.65
TiO_2	(0.01)	(0.01)	(0.01)	(0.01)	(0.01)	0.03	(0.02)	(0.01)	(0.01)	(0.01)	(0.01)
Al_2O_3	33.39	32.85	34.57	32.94	32.81	33.94	32.93	32.24	32.75	34.21	32.81
FeO	0.23	2.10	2.27	2.89	4.49	4.72	4.55	6.04	6.36	6.82	6.42
MnO	(0.02)	0.05	0.09	0.06	0.06	0.07	0.10	0.14	0.11	0.09	0.34
MgO	13.94	12.59	12.97	12.03	10.82	10.95	10.85	9.71	9.63	9.86	9.23
CaO	0.02	(0.01)	(0.02)	(0.01)	(0.01)	0.03	(0.02)	(0.01)	0.03	(0.01)	0.05
Na_2O	0.20	0.36	0.36	0.21	0.21	0.22	0.25	0.15	0.17	0.15	0.35
K_2O	0.00	0.00	0.00	(0.01)	(0.01)	0.04	(0.01)	(0.01)	0.00	0.02	(0.01)
P_2O_5	(0.01)	(0.01)	(0.02)	0.00	0.00	(0.06)	(0.02)	(0.02)	(0.03)	0.04	(0.02)
SO_3	0.02	(0.03)	(0.03)	(0.03)	0.03	0.02	0.06	(0.03)	(0.03)	(0.01)	0.04
Li_2O	0.00	0.009	n.d.	0.006	0.004	n.d.	0.035	0.005	0.01	n.d.	0.001
BeO	0.00	0.001	n.d.	0.001	<.001	n.d.	0.001	0.074	0.00	n.d.	0.000
B_2O_3	0.00	0.00	n.d.	0.00	<.001	n.d.	0.001	0.002	0.00	n.d.	0.001
H_2O	1.68	n.d.	n.d.	n.d.	n.d.	n.d.	n.d.	n.d.	1.47	n.d.	n.d.
Σ	98.85	96.55	100.55	96.69	96.68	99.00	97.13	96.10	98.63	100.54	96.92
Mg	2.092	1.919	1.900	1.837	1.663	1.647	1.663	1.513	1.486	1.471	1.431
Fe	0.019	0.180	0.187	0.248	0.387	0.398	0.391	0.528	0.551	0.571	0.558
Mn	0.000	0.004	0.007	0.005	0.005	0.006	0.009	0.012	0.010	0.008	0.030
Li	0.000	0.004	–	0.002	0.002	–	0.014	0.002	0.004	–	0.000
$\Sigma_{[6]}$	2.111	2.107	2.094	2.092	2.057	2.051	2.077	2.056	2.051	2.050	2.019
$Mg/\Sigma_{[6]}$	0.991	0.9108	0.9073	0.878	0.8084	0.8029	0.801	0.7361	0.7248	0.7178	0.7087
Al	3.961	3.959	4.003	3.976	3.987	4.035	3.990	3.972	3.996	4.035	4.021
Si	4.963	4.960	4.934	4.963	4.971	4.935	4.961	4.976	4.968	4.936	4.955
Be	0.000	0.000	–	0.000	0.000	–	0.000	0.019	0.000	–	0.000
$\Sigma_{[4]}$	8.924	8.919	8.937	8.938	8.958	8.970	8.950	8.967	8.964	8.972	8.975
$\Sigma - 11$	0.035	0.026	0.030	0.030	0.015	0.020	0.027	0.023	0.015	0.022	–0.006
Al/Si	0.7981	0.7981	0.8113	0.8011	0.8021	0.8177	0.8042	0.7983	0.8043	0.8175	0.8115
Na	0.039	0.071	0.069	0.042	0.042	0.043	0.050	0.030	0.034	0.029	0.071
K	0.000	0.000	0.000	0.000	0.000	0.005	0.000	0.000	0.000	0.003	0.000
Ca	0.002	0.000	0.000	0.000	0.000	0.003	0.000	0.000	0.003	0.000	0.006

Notes: Oxides in parentheses amount to less than one standard deviation after averaging. These are ignored in the calculated compositions, which are normalized to 18 oxygen atoms pfu. Sample numbers marked with an a denote single crystals obtained from cordierites annealed at 900 °C for 24 hours. 1 = 1997–1; 2 = 126231; 2a = 126231 (heated); 3 = Zimbabwe; 4 = 1960728; 4a = 1960728 (heated); 5 = 85131; 6 = NH1; 7 = GBL; 7a = GBL (heated); 8 = 94755; 9 = 111249; 9a = 111249 (heated); 10 = GREB370; 11 = 1997–2; 11a = 1997–2 (heated); 12 = g13994. n.d. = not determined.

The velocity scale was calibrated relative to 25 μm α-Fe foil using the positions certified for National Institute of Standards and Technology (NIST) standard reference material no. 1541; line widths of 0.28 mm/s for the outer lines of α-Fe were obtained at room temperature. The spectra were fitted to Lorentzian line shapes using the commercially available fitting program NORMOS written by R.A. Brand (distributed by Wissenschaftliche Elektronik GmbH, Germany).

Most cordierite spectra were fitted to a single Lorentzian doublet whose hyperfine parameters correspond to Fe^{2+} in octahedral coordination. Several spectra showed evidence for additional absorption, however, and these were fitted to an additional Lorentzian doublet. The hyperfine parameters of this doublet correspond most closely to tetrahedral Fe^{2+}, as suggested by Vance and Price (1984), and not channel Fe^{2+}, as suggested by Goldman and Rossman (1977). The two Fe^{2+} doublets accounted for all absorption and there was no evidence for Fe^{3+} in any of the spectra.

[2]For a copy of Tables 6 and 7, document item AM-00-061, contact the Business Office of the Mineralogical Society of America (see inside front cover of recent issue) for price information. Deposit items may also be available on the American Mineralogist web site (http://www.minsocam.org or current web address).

RESULTS AND DISCUSSION

EVOLUTION OF LATTICE CONSTANTS AS A FUNCTION OF COMPOSITION

As the unit-cell volume increases with increasing Fe content of the M-site, *a* and *b* increase, while **c** decreases (Fig. 1). Although both V and *b* are nearly linear functions of the compositional variable $[Mg]_M = Mg/(Mg + Fe + Mn + Li)$, both *a* and *c* deviate from linear behavior for small $[Mg]_M$. A slight increase in the *a* lattice constant is observable after removal of the volatile channel constituents. This increase causes a volume increase and, as only *a* increases, a significant increase in the distortion index, i.e., the orthorhombic distortion of the lattice. These changes are not observed in sample 111249, which is due to the minute water content of the natural sample. The behavior of the lattice constants on removal of volatile channel constituents can be related to the simultaneous presence of Na and H_2O in the natural cordierites. As Armbruster (1986) pointed out, Na is not only coordinated by the oxygen anions of the ring tetrahedra, but also by type II water. As H_2O is driven from the channels, Na is no longer restricted in its thermal movement along [001], leading to a strong increase in the U_{33} component of the thermal displacement tensor (Table 3). It follows that the Na-O bonds toward the ring O atoms weaken considerably on dehydration, resulting in the observed increase of strain and lattice volume.

TABLE 4—*Extended*

9	9a	10	11	11a	12
46.76	47.53	46.44	44.36	45.09	44.26
(0.02)	(0.01)	(0.01)	(0.01)	(0.03)	0.00
32.71	33.14	32.43	31.38	32.70	31.41
11.47	11.58	14.06	17.55	18.52	17.92
0.09	0.11	0.29	0.96	0.97	1.08
6.49	6.59	4.52	1.25	1.42	0.99
0.04	0.04	(0.01)	0.02	0.04	0.05
0.32	0.25	0.37	0.66	0.58	0.65
0.04	0.12	(0.01)	(0.01)	0.14	(0.01)
0.00	0.00	(0.07)	0.00	0.00	(0.02)
0.06	0.05	(0.02)	(0.02)	(0.02)	(0.03)
0.03	n.d.	0.115	0.156	n.d.	0.154
0.04	n.d.	0.006	0.00	n.d.	0.00
0.00	n.d.	0.001	0.003	n.d.	0.003
n.d.	n.d.	n.d.	1.43	n.d.	n.d.
98.05	99.42	98.36	97.80	99.51	96.624
1.017	1.019	0.715	0.206	0.228	0.164
1.008	1.004	1.248	1.626	1.668	1.661
0.008	0.010	0.026	0.090	0.088	0.101
0.013	–	0.049	0.069	–	0.069
2.046	2.032	2.039	1.991	1.985	1.995
0.4971	0.5012	0.3509	0.1035	0.1149	0.0822
4.053	4.049	4.057	4.096	4.151	4.103
4.916	4.928	4.930	4.913	4.857	4.905
0.010	–	0.002	0.000	–	0.000
8.979	8.977	8.989	9.009	9.008	9.008
0.025	0.010	0.028	0.000	–0.007	0.003
0.8245	0.8218	0.8230	0.8337	0.855	0.8365
0.065	0.050	0.076	0.142	0.121	0.140
0.005	0.016	0.000	0.000	0.019	0.000
0.005	0.004	0.000	0.002	0.005	0.006

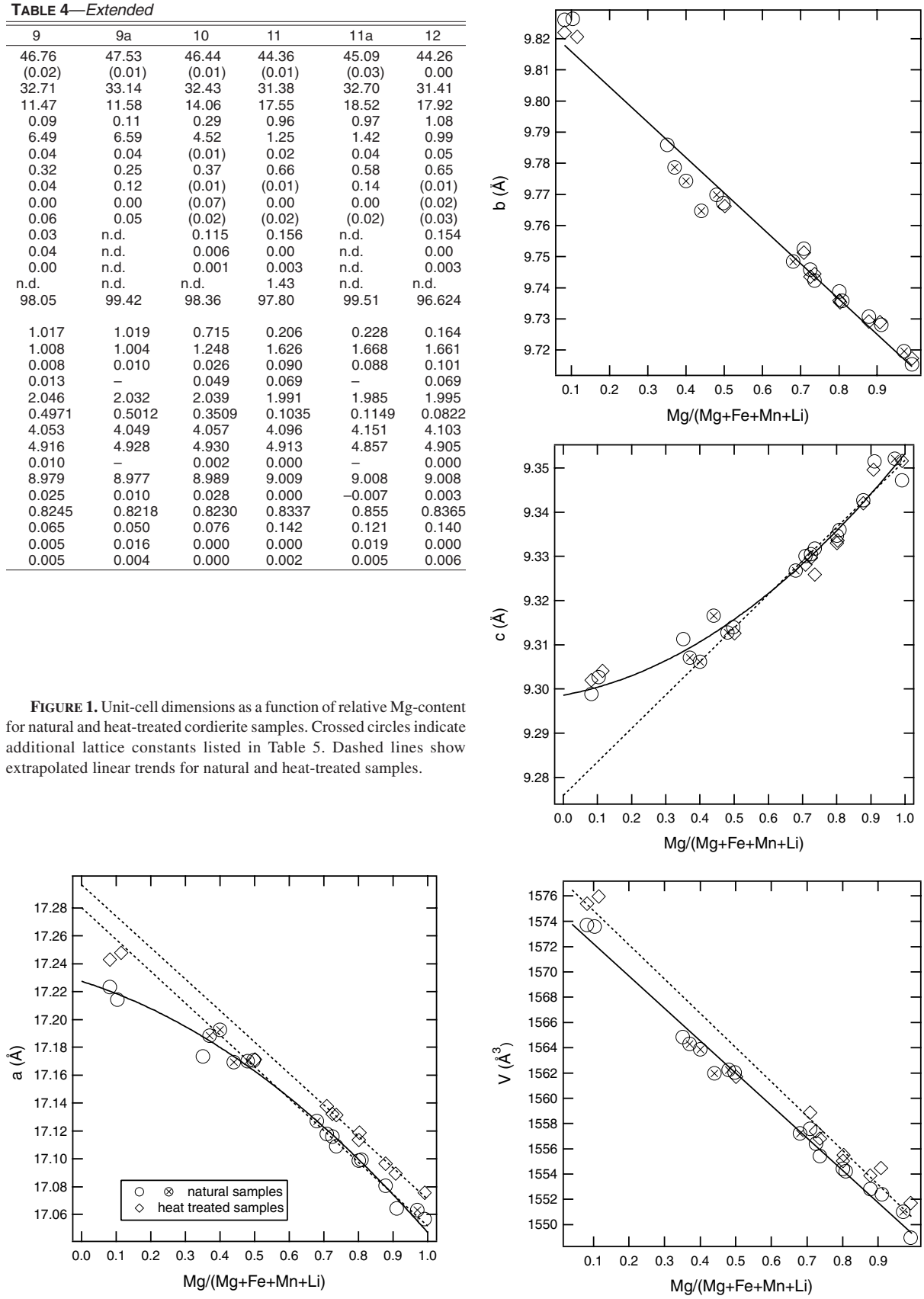

FIGURE 1. Unit-cell dimensions as a function of relative Mg-content for natural and heat-treated cordierite samples. Crossed circles indicate additional lattice constants listed in Table 5. Dashed lines show extrapolated linear trends for natural and heat-treated samples.

Structural properties

A general confirmation of the data quality can be obtained by comparison of Fe/Mg refinement on the M-site with the corresponding results of the EMPA. As shown in Figure 2, the two measurements are in satisfactory agreement for all examined crystals. The largest deviations occur in the Fe-rich cordierites that contain significant amounts of Li on the M-site (Table 4). In most cases the refined Na-content in (0,0,0) is in reasonably good agreement with the results of the EMPA.

The volume increase with increasing Fe-content correlates with the elongation of the mean ⟨M-O⟩ bond distance (Tables 6 and 7[2], Fig. 3). A clear systematic dependence on compositional variable is also seen in the mean bond length ⟨$T_1$1-O⟩, as shown in Figure 4. The linear fit to the data obtained for the natural samples is in good agreement with similar observations by Armbruster (1985c) (the dashed line in Fig. 4). The contraction of the mean $T_1$1-O bond length and accompanying systematic bond angle variations have been interpreted as being the result of structural requirements imposed by the increasing average size of the M-cation (Armbruster 1985c). The increasing size of the octahedral cation pushes the stacked pseudohexagonal rings of tetrahedra in opposite directions. This movement forces the T_1 to shrink and is responsible for the observed decrease in the **c**-lattice dimension. Such systematic bond length changes would require significant relaxation of individual cation-oxygen bonds if they were not accompanied by cation substitutions that can support these changes locally. The typical size of a tetrahedron occupied by Al^{3+} in an alumosilicate framework structure (about 1.749 Å for the mean bond length in anorthite) is consistent with the observed size of the $T_1$1-tetrahedron only toward the Fe-rich side of the solid solution. If the mean bond length is interpreted as the average arising from close packing of hard spheres, then any further increase toward the Mg-rich side of the solid solution requires substitution of larger ions for Al^{3+}. It is particularly striking that structure refinements of synthetic Mg-cordierite with nominal stoichiometry indeed show ⟨$T_1$1-O⟩ = 1.7495 Å (Rietveld refinement on neutron scattering data, M. Dove, personal communication). Besides, the $T_1$1-tetrahedron in pure Mg-cordierite is more strongly distorted than in the natural samples investigated here. The difference between bonds toward O13 and O11 atoms amounts to 0.037 Å, whereas this difference does not exceed 0.003 Å in the natural samples (Table 6). Using X-ray diffraction, Cohen et al. (1977) and Hochella et al. (1979) determined 0.003 Å for the same bond length difference in White Well cordierite (or 0.007 Å, using neutron diffraction). It can be concluded that the relatively large size of the "averaged" tetrahedron is needed to avoid large distortions in natural samples and that this large size is unsustainable in cordierite of composition $Mg_2Al_4Si_5O_{18}$.

The decrease of the mean tetrahedral bond length with increasing Fe-content should also occur in the $T_1$6-tetrahedron. However, symmetry requires this tetrahedron to remain undistorted. Figure 5 shows the average $T_1$6 bond length as a function of composition. From Shannon radii, the bond length for $Si^{[3]}O_4$ ⟨$T_1$6-O⟩ = 1.62 Å. The observed mean bond length is slightly larger than this expected value (~1.628 Å) and nearly constant across the solid solution, violating the trend of shrinking bond lengths in the T_1 tetrahedra.

From geometrical considerations, it could be expected that the degree of size reduction imposed by the structural framework is proportional to the pressure exerted on the individual tetrahedra by the "expanding" M-cation. The force that gives rise to this pressure is then twice as large at the $T_1$1-site, as two of these tetrahedra (but only one $T_1$6) are arranged around each octahedron. The surface of the tetrahedra is proportional to the square of the corresponding average bond length. Thus the ratio of the pressures experienced by the two tetrahedra would be

$$\frac{P_{T_1 1}}{P_{T_1 6}} = \frac{2\langle T_1 6 - O\rangle^2}{\langle T_1 1 - O\rangle^2} \approx 1.70$$

Hence, the gradient of the expected size variation of the $T_1$6-tetrahedron could be expected to amount to about 60% of the gradient observed in the $T_1$1-tetrahedron. A line showing the expected size increase, starting at 1.623 Å on the Fe-rich side, is drawn in Figure 5. The fact that the measured bond lengths plot above this expected trend for Fe-rich cordierites might be attributed to excess Al concentrations in these samples (cf. Table 4 and below).

Figures 6a and b show the mean bond length of the three ring tetrahedra as a function of composition. A significantly elongated bond length is observed at the $T_2$1 and $T_2$3 sites for the two Dolní Bory samples. This result is in agreement with previous refinements by Hochella et al. (1979). Otherwise the observed mean distances are close to 1.615 Å. The increase in T-O bond distance for the two Dolní Bory samples is clearly related to their excess Al-content. The excess mean bond length amounts to 0.003 Å (Table 6), whereas the difference between a T_1-tetrahedron containing Al and one containing Si is estimated to be 0.13 Å (see Table 8). Hence, the excess is 4/43 Al atoms, giving an Al/Si ratio of (4 + 4/43)/(5 – 4/43) = 0.834, which is close to the observed ratio in these samples. Thus we expect a lower degree of Al,Si ordering in these samples and a significant number of Al-O-Al bonds. The substitution of Al for Si is charge balanced by the presence of Na, which may well be localized adjacent to a particular Al-bearing tetrahedron. With a refined Na-content of 0.16 apfu, the excess Al-content of 0.093 apfu is overcompensated. The remaining positive charge is taken up by the substitution of 0.07 Li for a divalent cation.

The mean bond distance at the $T_2$6 site is within one e.s.d. of 1.74 Å for the majority of natural and heat-treated samples (Fig. 6b). This value is only slightly shorter than the 1.743 Å expected for an AlO_4 tetrahedron (cf. Table 8). The smaller values observed for the samples might indicate that minor amounts of Si substitute for Al on this site. The relative decrease in bond length is consistent with the increase relative to 1.62 Å seen in the ⟨$T_1$6-O⟩ mean bond length, suggesting Al,Si exchange between the $T_2$6 and $T_1$6 sites in these Fe-rich samples.

A direct refinement of Al,Si site occupancies on the tetrahedral sites is not feasible given their similar X-ray scattering powers. In turn, the scattering power of Mg is not very different from either of these two elements. However Fe and Mn

TABLE 5. Lattice constants of additional natural cordierite samples

Sample	Mg/(Mg + Fe + Mn)	*a* (Å)	*b* (Å)	*c* (Å)	*V* (Å³)	Δ=1.094(*a* − *b*√3)
129231	0.97	17.063(1)	9.7196(8)	9.3521(7)	1551.0(2)	0.24983
165	0.68	17.1271(4)	9.7484(2)	9.3268(2)	1557.2(1)	0.26516
366	0.48	17.1702(8)	9.7699(5)	9.3128(5)	1562.2(1)	0.27157
Lipari	0.44	17.1694(7)	9.7647(4)	9.3166(3)	1562.0(1)	0.28055
SN7289	0.37	17.188(2)	9.779(2)	9.307(1)	1564.3(3)	0.27481
SN7225	0.4	17.192(2)	9.7743(9)	9.3062(7)	1563.9(2)	0.28774

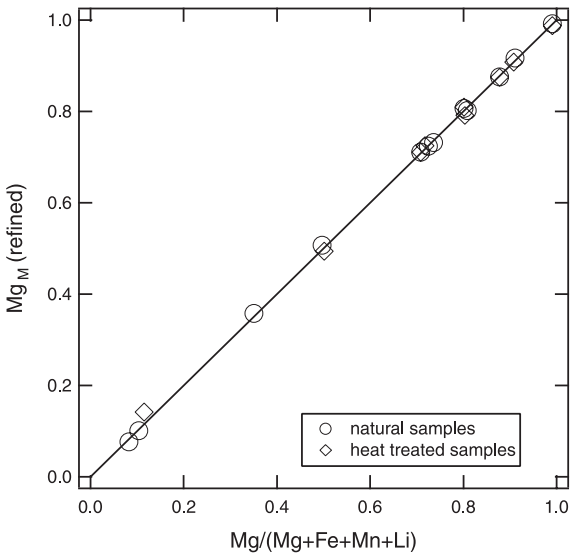

FIGURE 2. Refined Mg-occupancy in M plotted against relative Mg-content obtained from electron microprobe analysis. The straight line represents ideal agreement.

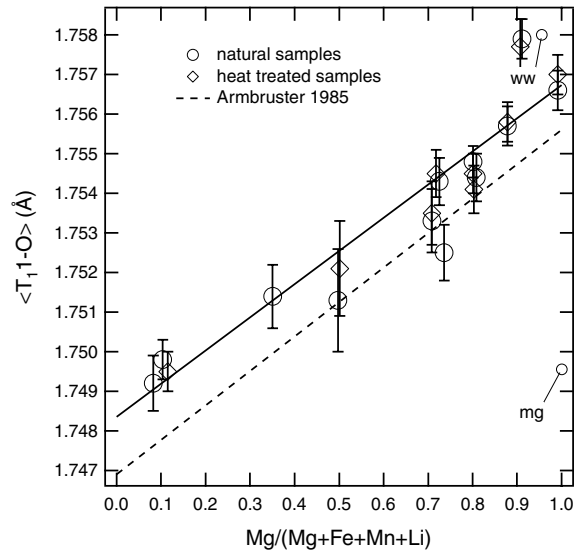

FIGURE 4. Mean distance ⟨$T_1$1–O⟩ as a function of Mg content, $[Mg]_M$ = Mg/(Mg + Fe + Mn + Li). ww = White Well cordierite, Cohen et al. 1977. Mg = synthetic low Mg-cordierite, M. Dove, personal communication.

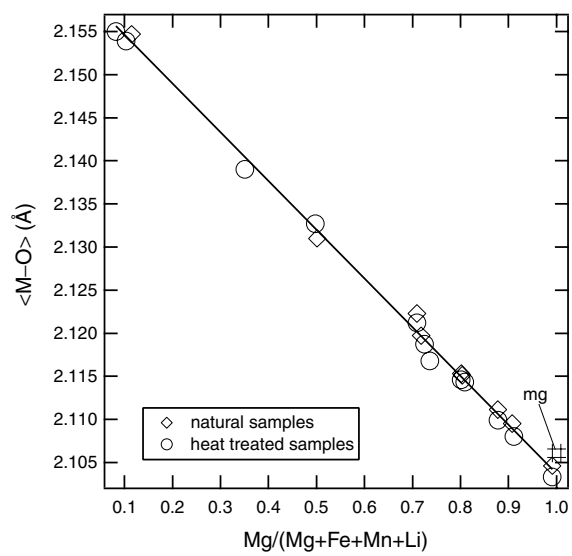

FIGURE 3. Mean octahedral distance ⟨M-O⟩ as a function of Mg content. Mg = synthetic low Mg-cordierite, M. Dove, personal communication.

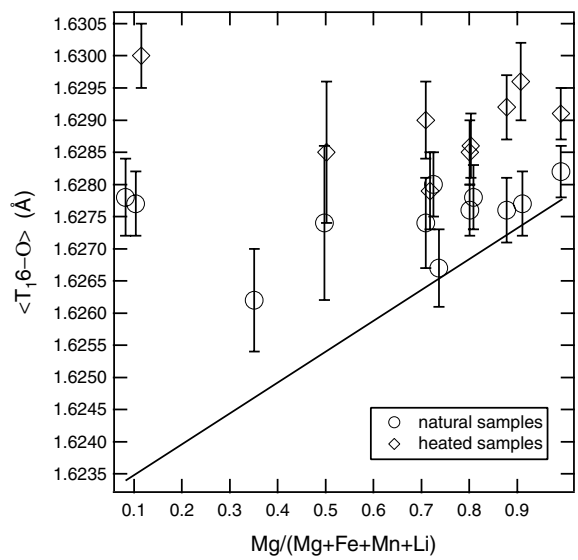

FIGURE 5. Mean distance ⟨$T_1$6–O⟩ as a function of Mg content, $[Mg]_M$ = Mg/(Mg + Fe + Mn + Li). The straight line represents the expected expansion of the site due to decreasing Fe-content in M (see text).

have significantly larger X-ray scattering factors. Hence Fe/Al and Fe/Si refinements were carried out on the $T_1$1 and $T_1$6 sites respectively, to obtain an estimate for the possible Fe-substitution on these sites. Attempts to place Fe on any of the other tetrahedral sites led to unstable refinements or to large correlations with the thermal displacement factors. The Fe site occupancies obtained are at or below 2% throughout (Table 2). In many cases, no significant Fe concentration was refinable in the $T_1$6 site, which was then assumed to be fully occupied by Si.

Quantification of site occupancies based on bond length consideration

To determine individual site occupancies, the cordierite structure can be approximated by a hard sphere model that relates measured bond length averages to the probability of finding individual cation-oxygen (M-O) bonds. If d_i is the mean distance associated with a particular coordination polyhedron *j* around a cation M_i, the average bond length over all such polyhedra (cation sites) is given by

$$\langle d \rangle_j = \sum_i p_{ij} d_i \qquad (1)$$

where p_{ij} is the probability of finding cation *i* occupying site *j*. We assume that all cation sites are completely filled, thus $\Sigma_i p_{ij} = 1$. One difficulty arising here is the fact that, in almost all cordierite samples examined, the sum of the structural cations is slightly larger than 11 (Table 4) when normalized to 18 oxygen atoms. To avoid unphysical overpopulation of sites in the model, the individual cation numbers were rescaled to a sum of 11. The reason for the enlarged cation sums might be related to the presence of oxygen defects, to protons binding to anions at the channel walls, or to analytical error.

The site occupancies p_{ij} can be determined by minimizing a set of equations if the individual, ideal polyhedral mean bond lengths, d_i, are known. Obtaining this number is relatively straightforward only for the tetrahedral Si-O bond exhibited by the $T_2$1,3 sites, as these distances are constant within measurement error for all but the Dolní Bory samples. Care has to be taken to distinguish tetrahedral bond lengths by the CN of participating oxygen anions. In the case of the T_2 sites, two oxygen atoms are 2-coordinated, while two others are 3-coordinated by two tetrahedral and one octahedral cation. The T_1 sites are exclusively coordinated by three-bonded oxygen atoms. For the ring tetrahedra, this situation is further complicated by the possible presence of Na at the center of the rings. An Na cation at (0,0,0) transforms a 2-coordinated oxygen atom to a 3-coordinated one, thereby slightly enlarging the mean distance of the associated tetrahedron (Armbruster 1986). This can be approximated using

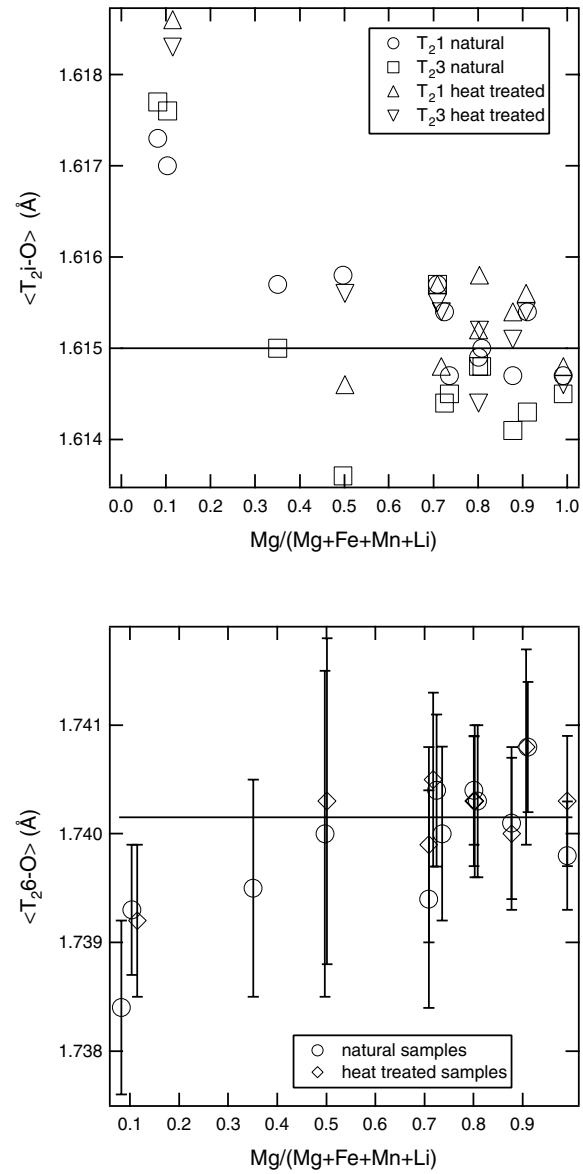

FIGURE 6. Mean distances ⟨T-O⟩ for the ring tetrahedra $T_2$1 and $T_2$3 (**a**) and for $T_2$6 (**b**). The horizontal lines represent the average of all data, with the exception of the Dolní Bory samples.

$$d_i[T_2]_{corr} = X_{Na} d_i[T_1] + (1 - X_{Na}) d_i[T_2] \qquad (2)$$

where $d_i[T_1]$ and $d_i[T_2]$ are the mean distances for tetrahedra with three-bonded and mixed two-and three-bonded coordination sphere, respectively. X_{Na} is the Na concentration in atoms per formula unit. As $X_{Na} << 1$, the amount of correction to the individual bond lengths of T_2 tetrahedra will be generally small.

TABLE 8. Individual polyhedral mean bond distances (Å) used in the calculations

CN 6				CN4						
Mg-O	Fe^{2+}-O	Mn^{2+}-O	Li-O	Al-O		Fe^{2+}-O	Mg-O	Si-O		Be-O
				T_1	T_2			T_1	T_2	T_1
2.104	2.165	2.215	2.144	1.7483	1.7433	1.99	1.955	1.6185	1.6135	1.628

An optimized set of individual bond distances is given in Table 8. First estimates were obtained from tabulated cation radii (Shannon 1976). The values were then adapted in a self consistent manner by applying separate correction factors to the octahedral and tetrahedral mean bond distances. The correction factor of 0.999 for the tetrahedral cations was obtained by comparison of ⟨Si-O⟩ = 1.6135 Å observed as the minimal value in the T_2 tetrahedra, with the corresponding value of 1.615 Å obtained from the appropriate sum of cation radii. The resulting mean distances for Si-O and Al-O are similar to those observed in anorthite (Megaw et al. 1962). In anorthite, a clear distinction between tetrahedra with different corner oxygen coordination numbers is hindered by the irregular coordination of the Ca-ion, but the global averages of the tetrahedral distances, 1.614 Å for Si-O and 1.749 Å for Al-O, are in good agreement with the values used here. The ⟨[4]Mg-O⟩ distance was adopted from experimental observations in Mg-Merrihueite (Khan et al. 1972). The mean octahedral bond distances were obtained by correcting the appropriate sums of cation radii by 1.0115; this correction factor was estimated using the value ⟨[6]Mg-O⟩ = 2.104 Å, refined by Khan et al. (1972) for the structure of Mg-Merrihueite. The corresponding distance from Shannon radii is 2.08 Å.

Given the experimental errors in the average bond distances, the bond length estimates given in Table 8 proved accurate enough to calculate Al,Si order parameters and minor Mg,Fe tetrahedral site occupancies using a hard sphere model of the cordierite structure. The calculated distances are generally within 0.003 Å of the observed distances.

The minimization function was constructed from a weighted sum of least squares, involving observed and calculated values of: (1) mean bond lengths $\langle d \rangle_j$, (2) Mg site occupancies in M, (3) Fe site occupancies in $T_1$1, (4) total abundance of Al and Si, and (5) charge balance. The total charge was calculated according to the number of oxygen atoms obtained after renormalization to 11 cations (see Table 9). Appropriate weights were chosen according to estimated measurement errors. Tetrahedral Mg was assumed to occupy the three T_1 sites in equal proportion, Fe was assumed to partition only onto the $T_1$1 (Geiger et al. 2000). Small Be concentrations, if present, also were assumed to occupy the $T_1$1 position (Armbruster 1986). Total Al and Si concentrations were allowed to slightly deviate from their measured values, to account for inaccuracies in the determination of the Al/Si ratio by EMPA. Si was assumed to partition only between the T_2 sites and $T_1$6. The refined parameters were the site occupancies for Al in $T_1$6, $T_2$1, $T_2$3, and $T_2$6 and the fractions of Fe and Mg occupying tetrahedral positions.

The results are summarized in Table 9. For those samples examined by Mössbauer-spectroscopy, the respective [4]Fe-contents are given for comparison. Order parameters were calculated according to the following equations, based on Al-site occupancies X:

$$Q_{T_1} = \frac{0.5X_{T_1 1} - X_{T_1 6}}{0.5X_{T_1 1} + X_{T_1 6}} \quad (3)$$

$$Q_{T_2} = \frac{2X_{T_2 6} - X_{T_2 1} - X_{T_2 3}}{2X_{T_2 6} + X_{T_2 1} + X_{T_2 3}} \quad (4)$$

$$\langle Q_{od} \rangle = \frac{1}{3}Q_{T_1} + \frac{2}{3}Q_{T_2} \quad (5)$$

$$Q_t = \frac{2X_{T_1 1} + X_{T_1 6} - 2X_{T_2 1} - 2X_{T_2 3} - 2X_{T_2 6}}{2X_{T_1 1} + X_{T_1 6} + 2X_{T_2 1} + 2X_{T_2 3} + 2X_{T_2 6}} \quad (6)$$

Q_{T_1} and Q_{T_2} determine the degree of order among the T_1 and T_2-tetrahedra, respectively. Weighting these two contributions by the relative number of tetrahedra gives $\langle Q_{od} \rangle$. Q_t measures the possible disproportion of Al between T_1 and T_2 sites.

The refined Fe^{2+} generally approaches the values obtained from Mössbauer spectroscopy within the estimated error. The total Fe-content increases from the top to the bottom of Table 9[4], thus the fraction of tetrahedral Fe is nearly constant across

TABLE 9. Tetrahedral Fe-content obtained from Mössbauer spectroscopy and results of the bond distance refinements

Sample	T (°C)	[4]Fe (%)		[4]Mg (%)	Al/Si		Q_{od}			Q_t	O_n
		Mössbauer	XRD		EMPA	refined	T1	T2	$\langle Q_{od} \rangle$		
1997-1	–	n.d.	63(33)	4.4(3)	0.7981	0.7969	1.00	0.970	0.980	–0.02	17.95
	900	n.d.	70(8)	4.4(1)	0.7981	0.7969	0.979	0.972	0.975	–0.02	17.94
126231	–	11(3)	15(5)	3.9(5)	0.7982	0.7973	0.968	0.975	0.973	–0.02	17.96
	900	n.d.	11(5)	3.8(5)	0.8113	0.8101	0.901	0.967	0.945	–0.02	17.95
Zimb	–	5(2)	9(6)	3.4(8)	0.8011	0.8009	0.929	0.976	0.960	–0.01	17.95
	900	n.d.	4(4)	4.1(5)	0.8011	0.8001	0.928	0.972	0.957	–0.01	17.95
1960728	–	0(2)	4(3)	2.3(8)	0.8021	0.8015	0.854	0.983	0.940	0.00	17.98
	900	n.d.	2(2)	2.4(4)	0.8176	0.8169	0.835	0.969	0.924	0.00	17.97
85131	–	n.d.	8(2)	2.3(5)	0.8043	0.7908	0.881	0.976	0.944	–0.02	17.95
	900	n.d.	7(2)	2.6(5)	0.8043	0.8033	0.846	0.980	0.935	0.00	17.96
NH1	–	n.d.	3(3)	2(1)	0.7982	0.7970	0.868	0.982	0.944	0.00	17.96
GBL	–	0(2)	4(2)	1.8(9)	0.8044	0.8038	0.813	0.987	0.929	0.01	17.98
	900	n.d.	5(3)	1(1)	0.8175	0.8165	0.787	0.975	0.912	0.00	17.96
94755	–	n.d.	3(2)	0.2(7)	0.8115	0.8116	0.768	0.976	0.907	0.02	18.01
	900	n.d.	3(2)	0(1)	0.8115	0.8116	0.729	0.983	0.898	0.01	18.01
111249	–	0(2)	3(1)	0.7(1)	0.8245	0.8234	0.764	0.969	0.901	0.00	17.96
	900	n.d.	2(1)	1.7(1)	0.8216	0.8206	0.771	0.971	0.905	0.00	17.96
Greb370	–	0(2)	2(1)	0.4(1)	0.8229	0.8219	0.786	0.967	0.907	0.00	17.96
19972	–	n.d.	0.0	0.0	0.8337	0.8336	0.752	0.952	0.886	0.01	17.98
	900	n.d.	1(1)	10(7)	0.8546	0.8532	0.747	0.925	0.866	-0.01	17.94
G13994	–	n.d.	0.0	0.0	0.8365	0.8363	0.748	0.945	0.879	0.01	17.99

the solid solution. Mg appears to occupy tetrahedral positions mainly in Mg-rich cordierites, following the expansion of the T_1 tetrahedra. Maximum Mg-contents of 4% or 0.08 atoms pfu can be expected according to the calculations. This result is in agreement with the excess Mg content seen in the chemical analysis of the most Mg-rich sample (Table 4). Note that this postulated concentration of $^{[4]}$Mg is about four times larger than the largest observed $^{[4]}$Fe concentration.

The degree of Al,Si ordering decreases slightly in Fe-rich samples. Except for the most Fe-rich samples all cordierites exhibit nearly complete order among the T_2 sites, whereas Al,Si ordering among the T_1 sites falls to levels of only 75% toward the Fe-rich side of the solid solution. Mg-rich cordierites, on the other hand, appear to be almost fully ordered. The measurement error of Q_{od} can be estimated as about 3%. Within this error, no significant change in the order parameter is observed upon heating to 900 °C. Regarding Q_i, no significant deviation from equal distribution of Al across the T_1 and T_2 sites is observable.

Order parameter and macroscopic strain

In Figure 7, Q_{od} is plotted as a function of

$$e_s = \frac{a - b\sqrt{3}}{a + b\sqrt{3}} = \frac{e_1 - e_2}{e_1 + e_2 + 2} \qquad (7)$$

In contrast to the commonly cited distortion index (Δ), the parameter e_s can be rigorously defined based on the orthorhombic strain components e_1 and e_2, that define the orthorhombic shear strain $e_o = (e_1 - e_2)$ (Carpenter et al. 1998). If the shear strain is homogeneous, $e_1 + e_2 = 0$ and $e_s = e_o/2$.

It is well known that the magnitude of the distortion index depends on the degree of order, but also on the chemical composition (Selkregg and Bloss 1980). Similarly, the shear strain does not immediately yield a clear correlation with the order parameter. Because of its negligible water content, sample 111249, for example, plots with the dehydrated samples rather than with the natural samples in Figure 7. A calibration of Q_{od} as a function of shear strain e_s therefore requires an exact knowledge of compositional parameters such as H_2O, Na, and Fe/Mg content. All these variables are known for the three natural samples 1997-1, GBL, and 1997-2, and for the heat-treated samples, which contain no H_2O.

Selkregg and Bloss (1980) approximated the distortion index empirically as a linear function of octahedral ionic radius, Na-content, and H_2O-content. Based on such an approximation, the contribution of Al,Si ordering could then be accounted for by addition of a further linear contribution arising from variation of Q_{od} (Putnis et al. 1987). However, Al,Si ordering is expected to be the only symmetry breaking property in cordierite. Any linear dependence of e_s on a compositional variable X_i would imply that X_i behaves as a conjugate field to $(e_1 - e_2)$ and hence to Q_{od} (Redfern et al. 1989). Thus, in effect, Fe, Na, H_2O, etc., would generate the equivalent of an external field with the same symmetry properties as Q_{od}, and ordering would be either enhanced or suppressed, depending on the sign of the coupling between X_i and $(e_1 - e_2)$.

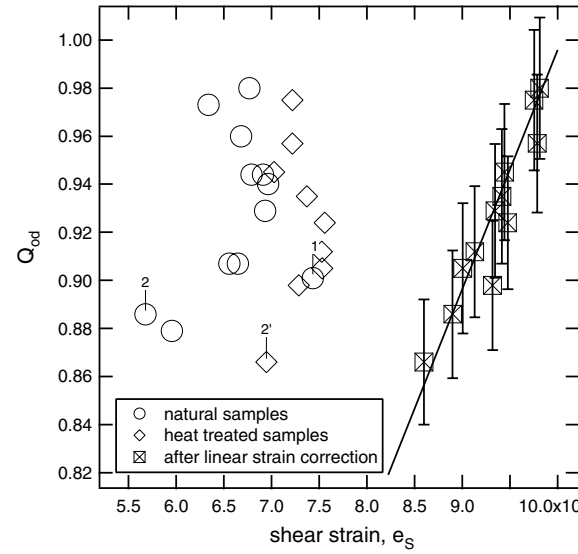

FIGURE 7. Plot of the order parameter Q_{od} as a function of shear strain, e_s, for natural and heat treated samples and for selected samples after linear strain correction (see text). (1) Marks the almost H_2O free, natural sample 111249. (2,2') mark sample 1997-2 before and after dehydration. The strain errors are in the order of the symbol size. The straight line represents $Q_{od} = -e_s(C_{11}^0 - C_{12}^0)/\lambda_q$.

The form of the free energy expansion describing this behavior is

$$\begin{aligned} G = {} & G_L(Q) + \lambda_q(e_1 - e_2)Q + \lambda_z e_3 Q^2 + \lambda_v(e_1 + e_2)Q^2 \\ & + \sum_i \left[\lambda_{x_i,s}(e_1 - e_2)^n + \lambda_{x_i,z} e_3 + \lambda_{x_i,v}(e_1 + e_2)\right] X_i \\ & + \frac{1}{4}\left(C_{11}^0 - C_{12}^0\right)(e_1 - e_2)^2 + \frac{1}{4}\left(C_{11}^0 + C_{12}^0\right)(e_1 + e_2)^2 \end{aligned} \qquad (8)$$

with n = 1. $G_L(Q)$ is the free energy contribution arising from Al,Si ordering, e_3 is the z-component of the orthorhombic strain, $(e_1 + e_2)$ measures the inhomogeneity of the orthorhombic distortion, X_i denote the compositional variables, and C_{11}^0 and C_{12}^0 are bare elastic constants. If the field effect of X_i is to enhance $(e_1 - e_2)$, the equilibrium stability field of hexagonal cordierite would be suppressed. If X_i acts in opposition to $(e_1 - e_2)$, the hexagonal to orthorhombic transition temperature will be reduced.

In a stress-free crystal, G is in equilibrium with respect to $(e_1 - e_2)$, hence it follows that

$$\frac{e_1 - e_2}{2} = -\frac{\lambda_q Q_{od} + \sum_i \lambda_{X_i,s} X_i}{C_{11}^0 - C_{12}^0} \qquad (9)$$

To obtain the calibration of Q as a function of e_s, the parameters in Equation 9 were determined by fitting $(e_1 - e_2)/2$ to the experimental data e_s. [It can be safely assumed that $(e_1 + e_2)$ is small, hence $e_s = (e_1 - e_2)/2$]. The compositional variables used were X_{Na}, X_{H_2O} (both in atoms pfu), and the relative Mg-concentration $[Mg]_M$. If X_{Na} was not available from microprobe analysis, the value determined by XRD site refinement was used instead (cf. Table 3). Addition of a further term,

$\lambda_{Na,H_2O}X_{H_2O}X_{Na}$, significantly improved the fit. This coupling between Na and H_2O content accounts for the increased thermal movement of Na caused by the absence of type II H_2O molecules, hence for a diminished interaction of Na with the coordinating oxygen atoms of the cordierite structure in dehydrated samples. Appropriate values of C_{11}^0 and C_{12}^0 have been determined by Toohill et al. (1999). Using the best-fit parameters, the order parameter in this approximation can be formulated as

$$Q_{od} = -\frac{(C_{11}^0 - C_{12}^0)}{\lambda_q} e_s^c \quad (10)$$

$$e_s^c = \frac{e_1 - e_2}{2} + \frac{\lambda_{Na}}{C_{11}^0 - C_{12}^0} X_{Na} + \frac{\lambda_{Mg}}{C_{11}^0 - C_{12}^0}[Mg]_M + \frac{\lambda_{H_2O}}{C_{11}^0 - C_{12}^0} X_{H_2O} + \frac{\lambda_{Na,H_2O}}{C_{11}^0 - C_{12}^0} X_{Na,} X_{H_2O} \quad (11)$$

with the parameters λ_q = –1.141(6) GPa, λ_{Na} = 1.36(6) GPa/mol, λ_{Mg} = 0.199(4) GPa, λ_{Na,H_2O} = 1.14(12) GPa/mol^2, and λ_{H_2O} = 0.126(7) GPa/mol and $C_{11}^0 - C_{12}^0$ = 113.6 GPa (cf. Toohill et al. 1999). Values in parentheses denote the approximate errors of the parameters. In Figure 7, Q_{od} is plotted as a function of the reduced strain e_s^c, demonstrating the linear correlation between strain and order parameter. Note that λ_q and the compositional coupling constants are of opposite sign. Thus the presence of Na and H_2O, as well as the absence of Fe, stabilize the hexagonal, disordered phase, via a decrease of the strain in Equation 9.

An alternative to the above considerations is to assume that X_i behaves as a normal compositional variable without symmetry properties. In this case the lowest order coupling permitted by symmetry between $(e_1 - e_2)$ and X_i has the form $\lambda_{xi,s}(e_1 - e_2)^2 X_i$, i.e., n = 2 in Equation 8. It follows then that

$$\frac{e_1 - e_2}{2} = \frac{-\lambda_q Q}{4\sum_i \lambda_{X_i} X_i + (C_{11}^0 - C_{12}^0)} \quad (12)$$

It is obvious that the compositional variables in Equation 12 cannot generate strain independently of Q, contrary to the assumptions that lead to Equation 9. If n = 2, only the elastic response of the cordierite structure with respect to Al,Si ordering is modified by the impurities. Using the best-fit parameters now yields the equation

$$Q_{od} = a\frac{e_1 - e_2}{2} \quad (13)$$

$$a = \frac{4\lambda_{Na}X_{Na} + 4\lambda_{Mg}[Mg]_M + 4\lambda_{H_2O}X_{H_2O} + 4\lambda_{Na,H_2O}X_{Na}X_{H_2O} + C_{11}^0 - C_{12}^0}{-\lambda_q} \quad (14)$$

where λ_q = –1.176(5) GPa, λ_{Na} = 58(3) GPa/mol, λ_{Mg} = 7.4(2) GPa, λ_{Na,H_2O} = 82(5) GPa/mol^2, and λ_{H_2O} = 4.6(3) GPa/mol. In Figure 8, this calculated order parameter is compared with the observed values. Note that all terms contributing to the numerator in Equation 14 are positive, thus increasing the relevant shear rigidity of the cordierite structure. Regarding the properties of the solid solution, this rigidity is at a maximum for pure Mg-cordierite.

With the data that is available a decision cannot be reached as to which of the two order parameter calibrations, Equations 10–11 or Equations 13–14, is formally correct. Both models fit the data with similar accuracy. Moreover, the value of the exponent n = {1,2} might depend on the particular impurity in question, leading to a combination of both models. Further refinement of the strain calibration, using a wider variety of order parameters obtained via heat treatment, will be the subject of a separate paper (Malcherek et al., in preparation).

The occurrence of macroscopic strain, cation substitution, and partial Al,Si disorder has to be seen in context to explain the properties of the solid solution. Charge balance for the substitution of divalent cations for Al^{3+} is provided by introduction of Na^+ into the channels or by substitution of an additional Al^{3+} by Si^{4+}. The latter substitution is nearly volume conserving, as the replacement of Al by the larger cations Mg^{2+} or Fe^{2+} requires space similar to that freed by the replacement of Al by Si. On the other hand, the increasing Al/Si ratio with increasing Fe-content (Table 4) suggests that the substitution $Al^{3+} + Na^+ = Si^{4+}$ dominates in Fe-rich cordierites. The introduction of Na into the Ch2-sites and the introduction of excess Al both lower the orthorhombic lattice distortion. As the lattice distortion increases with increasing Fe-content, such a substitution scheme supports the elastic stability of Fe-cordierite at the cost of energetically unfavorable Al-O-Al neighborhoods. However, if the occurrence of such bonds can be restricted to T_2 tetrahedra, as the excess Al in cordierites suggests, Na might have a stabilizing effect as it would bind to the bridging oxygen atom, i.e., either $O_2$6 or $O_2$1 (Armbruster 1986).

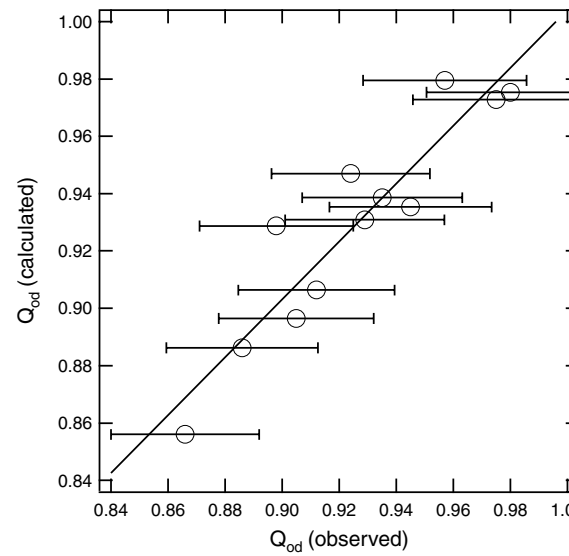

FIGURE 8. Calculated order parameter, based on Equation 13, plotted as a function of the observed values. The horizontal error bars correspond to an estimated error of 3% in the measured order parameters.

CONCLUDING REMARKS

It has been shown that the observed mean bond distances in a suite of natural and heat-treated cordierite samples are, to a good approximation, consistent with a simple hard sphere model of the cordierite structure. This model requires the introduction of minor amounts of Fe^{2+} and Mg cations into the tetrahedral framework. Whereas direct spectroscopic evidence confirms the presence of Fe in tetrahedral coordination, the possibility of tetrahedrally coordinated Mg is inferred from chemical analysis showing excess Mg-content, from the structural similarity to Mg-merrihueite, and from the favorable size of Mg^{2+} compared to Fe^{2+} in tetrahedral coordination. Almost complete Al,Si order is found in Mg-rich natural samples, whereas Fe-rich samples exhibit lesser Al,Si order due to an increased Al/Si ratio. Correlation of the order parameter with the orthorhombic distortion is confirmed.

These observations underline the marked difference between strictly stoichiometric, synthetic cordierites and those occurring in nature. The presence of minor tetrahedral cations appears to be stabilizing the cordierite structure with respect to local distortions. The mean $T_1$1-O distance ranges between 1.756 and 1758 Å, in all natural Mg-cordierites it is significantly smaller in synthetic cordierite, as the ideal Al-O distance is below 1.75 Å. These smaller tetrahedra can only match the edge-sharing octahedra at the cost of a strongly distorted tetrahedron. By reverting to either (1) correlated local distortions or (2) randomly distributed Al and Si on the three T_1 sites, the mismatch between tetrahedra and octahedra in the M-layers may be reduced. The latter scenario might explain why synthetic cordierite first crystallizes in the hexagonal, disordered modification, whereas the former might be realized in the modulated cordierites that develop at the onset of Al,Si ordering in synthetic cordierites (Putnis et al. 1987). During later stages the mismatch could be balanced by Al/Si exchange between the T_2 and the $T_1$6 sites, thus giving rise to a finite, positive value of Q_t and $Q_{od} << 1$ in synthetic samples (Vinograd 1996). In natural samples the structure can be stabilized by filling the T_1 sites with larger cations at appropriate distances. The refined tetrahedral Mg-concentration of 0.08 atoms pfu in Mg-cordierite would, on average, require the substitution of Mg for one Al in every third unit cell. Whether such substitutions can give rise to further ordering processes among the minor Fe and Mg cations remains to be investigated.

The particular crystal chemistry of the Fe-cordierites from the Dolní Bory locality might not be of general significance, because of their high contents of Na and Li (Černý et al. 1997). However, it is important to stress that the orthorhombic distortion of cordierite increases with Fe-content, and a possible explanation for the scarce occurrence of Fe-cordierite in nature and its narrow stability field in experiments might be provided by the necessity to lessen the orthorhombic distortion by other means, i.e., a high Al/Si ratio and large concentrations of Na in the Ch2 extra-framework site. Provided sufficient concentrations of Na are present, a high H_2O content could also indirectly lower the orthorhombic distortion.

ACKNOWLEDGMENTS

The contribution of unpublished results on the structure of synthetic Mg-cordierite by M. Dove is gratefully acknowledged. The help of S.B. Reed with the electron microprobe analysis is greatly appreciated. This study would not have been possible without the generous help of numerous people who provided samples: T. Armbruster, F. Bea, G.A. Chinner, C. Francis, N. Harris, T.J.B. Holland, D. Perkins, A. Pring, and J.A. Speer. Comments by T. Armbruster helped to improve the manuscript. Financial support by European Union TMR network ERB-FMRX-CT97-0108 and by Italian MURST (project "Relation between structure and properties in minerals: analysis and applications").

REFERENCES CITED

Armbruster, T. (1985a) Ar, N_2, and CO_2 in the structural cavities of cordierite, an optical and X-ray single-crystal study. Physics and Chemistry of Minerals, 12, 233–245.

———(1985b) Crystal structure refinement, Si,Al-ordering, and twinning in "pseudo-hexagonal" Mg-cordierite. Neues Jahrbuch Mineralogie Monatshefte, p. 255–267.

———(1985c) Fe-rich cordierites from acid volcanic rocks, an optical and X-ray single-crystal study. Contributions to Mineralogy and Petrology, 91, 180–187.

———(1986) Role of Na in the structure of low-cordierite: A single-crystal X-ray study. American Mineralogist, 71, 746–757.

Armbruster, T. and Bloss, F.D. (1982) Orientation and effects of channel H_2O and CO_2 in cordierite. American Mineralogist, 67, 284–291.

Carpenter, M.A., Salje, E.K.H., and Graeme-Barber, A. (1998) Spontaneous strain as a determinant of thermodynamic properties for phase transitions in minerals. European Journal of Mineralogy, 10, 621–69 1.

Černý, P., Chapman, R., Schreyer, W., Ottolini, L., Bottazzi, P., and McCammon, C.A. (1997) Lithium in sekaninaite from the type locality, Dolní Bory, Czech republic. Canadian Mineralogist, 35, 167–173.

Chinner, G.A. (1962) Almandine in thermal aureoles. Journal of Petrology, 3, 316–340.

Cohen, J., Ross, F., and Gibbs, G. (1977) An X-ray and neutron diffraction study of hydrous low cordierite. American Mineralogist, 62, 67–78.

Finger, L.W., Cox, D.E., and Jephcoat, A.P. (1994) A correction for powder diffraction peak asymmetry due to axial divergence. Journal of Applied Crystallography, 27, 892–900.

Geiger, C.A., Armbruster, T., Khomenko, V., and Quartieri, S. (2000) Cordierite I: The coordination of Fe^{2+}. American Mineralogist, 85, 1255–1264.

Gibbs, G.V. (1966) The polymorphism of cordierite I: the crystal structure of low cordierite. American Mineralogist, 51, 1068–1087.

Goldman, D.S. and Rossman, G.R. (1977) Channel constituents in cordierite. American Mineralogist, 62, 1144–1157.

Hawthorne, F.C., Kimata, M., Černý, P., Ball, N., Rossman, G.R., and Grice, J.D. (1991) The crystal chemistry of the milarite-group minerals. American Mineralogist, 76, 1836–1856.

Hochella, M., Brown, G., Ross, F., and Gibbs, G. (1979) High temperature crystal chemistry of hydrous Mg- and Fe-cordierites. American Mineralogist, 64, 337–351.

Khan, A.A., Baur, W.H., and Forbes, W.C. (1972) Synthetic magnesian merrihueite, dipotassium pentamagnesium dodecasilicate: a tetrahedral magnesiosilicate framework crystal structure. Acta Crystallographica, B28, 267–272.

Larson, A.C. and Von Dreele, R.B. (1994) General structure analysis system (GSAS). Tech. Rep. LAUR B6-748, Los Alamos National Laboratory Report, Los Alamos, New Mexico.

Meagher, E.P. and Gibbs, G.V. (1977) The polymorphism of cordierite: II. The crystal structure of indialite. Canadian Mineralogist, 15, 43–49.

Megaw, H.D., Kempster, C.J.E., and Radoslovich, E.W. (1962) The structure of anorthite, $CaAl_2Si_2O_8$. II. Description and Discussion. Acta Crystallographica, 15, 1017–1035.

Ottolini, L., Bottazzi, P., and Vannucci, R. (1993) Quantification of lithium, beryllium and boron in silicates by secondary ion mass spectrometry using conventional energy filtering. Analytical Chemistry, 65, 1960-1968

Ottolini, L., Bottazzi, P., Zanetti, A., and Vannucci, R. (1995) Determination of hydrogen in silicates by secondary ion mass spectometry. The Analyst, 120, 1309–1314.

Pereira, M.D. and Bea, F. (1994) Cordierite-producing reactions in the PenaNegra complex, Avila Batholith, Central Spain—the key role of cordierite in low-pressure anatexis. Canadian Mineralogist, 32,763–780.

Povondra, P., Cech, F., and Burke, E. (1984) Sodian-beryllian cordierite from Gammelmorskärr, Kemiö island, Finland, and its decomposition products. Neues Jahrbuch Mineralogie Monatshefte, p. 125–136.

Povondra, P. and Langer, K. (1971a) A note on the miscibility of magnesia-cordierite and beryl. Mineralogical Magazine, 38, 523–526.

———(1971b) Synthesis and some properties of sodium-beryllium-bearing cordierite, $Na_xMg_2(Al_{4-x}Be_xSi_5O_{18})$. Neues Jahrbuch Mineralogie Abhandlungen, 116, 1–19.

Putnis, A. (1980) The distortion index in anhydrous Mg-cordierite. Contributions to Mineralogy and Petrology, 74, 135–141.

Putnis, A., Salje, E., Redfern, S., Fyfe, C., and Strobl, H. (1987) Structural states of Mg-cordierite I: Order parameters from synchrotron X-ray and NMR data. Physics and Chemistry of Minerals, 14, 446–454.

Redfern, S.A.T., Salje, E., Maresch, W., and Schreyer, W. (1989) X-ray powder-diffraction and infrared study of the hexagonal to orthorhombic phase transition in K-bearing cordierite. American Mineralogist, 74, 1293–1299.
Schreyer, W. (1985) Experimental studies on cation substitutions and fluid incorporation in cordierite. Bulletin de Minéralogie, 108, 273–291.
Schreyer, W. and Schairer, J.F. (1961) Compositions and structural states of anhydrous Mg-cordierites: a reinvestigation of the central part of the system MgO-Al_2O_3-SiO_2. Journal of Petrology, 2, 324–406.
Selkregg, K.R. and Bloss, F.D. (1980) Cordierites: compositional controls of Δ, cell parameters, and optical properties. American Mineralogist, 65, 522–533.
Shannon, R.D. (1976) Revised effective ionic radii and systematic studies of interatomic distances in halides and chalcogenides. Acta Crystallographica, A32,751.
Sheldrick, G.M. (1997) Shelx-97. Technical report, Universität Göttingen, Germany.
Speer, J.A. (1982) Metamorphism of the pelitic rocks of the Snyder Group in the contact aureole of the Kiglapait layered intrusion, Labrador: effects of buffering partial pressures of water. Canadian Journal of Earth Science, 19, 1888–1909.
Toohill, K., Siegesmund, S., and Bass, J.D. (1999) Sound velocities and elasticity of cordierite and implications for deep crustal seismic anisotropy. Physics and Chemistry of Minerals, 26, 333–343.
Vance, E-R. and Price, D.C. (1984) Heating and radiation effects on optical and Mössbauer spectra of Fe-bearing cordierites. Physics and Chemistry of Minerals, 10, 200–208.
Vinograd, V.L. (1996) Computer simulations of Al-Si disorder in synthetic cordierites: Configurational entropy constrained by ^{29}Si NMR data. Physics and Chemistry of Minerals, 23, 391–401.
Vry, J., Brown, P., and Valley, J. (1990) Cordierite volatile content and the role of CO_2 in high-grade metamorphism. American Mineralogist, 75, 71–88.
Wallace, J.H. and Wenk, H.R. (1980) Structure variation in low cordierites. American Mineralogist, 65,96–111.

MANUSCRIPT RECEIVED JANUARY 12, 2000
MANUSCRIPT ACCEPTED AUGUST 14, 2000
PAPER HANDLED BY JEFFREY E. POST

APPENDIX: SAMPLE DESCRIPTION

1997-1. Salem, Tamil, Naidu, SE-India. With Qz, albite. Cordierite crystals frequently contain thin hematite lamellae. (Cambridge mineral collection. Sample originally donated by N. Harris)

129825. Manik Ganga, Sri Lanka. Part of large colorless/pale violet single crystal. (Harvard University mineral collection)

126231. Tanzania. Part of large blue single crystal. (Harvard University mineral collection)

Zimb. Zimbabwe. With Qz, apatite. (Sample provided by T.J.B. Holland)

1960728. Orijarvi, Finland. (Cambridge Mineral Collection)

85131. Mt. Bity, Madagaskar. Blue crystals. (Harvard University mineral collection)

GBL. Great Bear Lake, Canada. Contains thin oriented, lamellaer inclusions of dark-greenish color. Described by Vry et al. (1990) (Sample provided by D. Perkins)

94755. Tincup mining district, Rawlins, Wyoming. Contains finely dispersed unknown alterations. (Harvard University mineral collection)

165. Hornfels, Glen Clova, Scotland. Described by Chinner (1962). (Cambridge, Harker number 82917)

366. Hornfels, Glen Muick, Scotland. Described by Chinner (1962). (Cambridge, Harker number 82888)

111249. Cerro del Hoyazo, Spain. (Cambridge Harker collection)

Lipari. Italy. With spinel inclusions, feldspar. Described by Armbruster (1985c). (Sample provided by T. Armbruster)

SN7289. Snyder Bay, Labrador. With Qz, potassium feldspar, sillimanite. Geological setting described by Speer (1982). (Sample provided by J.A. Speer)

SN7225. Snyder Bay, Labrador. With Qz, potassium feldspar, sillimanite and andalusite. Geological setting described by Speer (1982). (Sample provided by J.A. Speer)

Greb370. Pena Negra Complex, Spain. Geological setting described by Pereira and Bea (1994). (Sample provided by F. Bea)

1997-2. Dolní Bory, Czech Republic. (Cambridge mineral collection)

G13994. Dolní Bory, Czech Republic. (S. Australian museum)